Effect of the loading frequency on the sand liquefaction behaviour in cyclic triaxial tests

Zhehao Zhu, Feng Zhang, Qingyun Peng, Jean Claude Dupla, Jean Canou, Gwendal Cumunel, Evelyne Foerster

▶ **To cite this version:**

Zhehao Zhu, Feng Zhang, Qingyun Peng, Jean Claude Dupla, Jean Canou, et al.. Effect of the loading frequency on the sand liquefaction behaviour in cyclic triaxial tests. Soil Dynamics and Earthquake Engineering, 2021, 147, pp.106779. 10.1016/j.soildyn.2021.106779 . hal-04313255

HAL Id: hal-04313255
https://hal.science/hal-04313255v1

Submitted on 22 Jul 2024

HAL is a multi-disciplinary open access archive for the deposit and dissemination of scientific research documents, whether they are published or not. The documents may come from teaching and research institutions in France or abroad, or from public or private research centers.

L'archive ouverte pluridisciplinaire **HAL**, est destinée au dépôt et à la diffusion de documents scientifiques de niveau recherche, publiés ou non, émanant des établissements d'enseignement et de recherche français ou étrangers, des laboratoires publics ou privés.

Distributed under a Creative Commons Attribution - NonCommercial 4.0 International License

Version of Record: https://www.sciencedirect.com/science/article/pii/S0267726121002013
Manuscript_24410b21019a0a9321a3c47561c3067a

Effect of the loading frequency on the sand liquefaction behaviour in cyclic triaxial tests

Zhehao Zhu[a,b], Feng Zhang[a,*], Qingyun Peng[a], Jean-Claude Dupla[a], Jean Canou[a], Gwendal Cumunel[a], Evelyne Foerster[b]

[a]Ecole des Ponts ParisTech, Laboratoire Navier, 6-8 av. Blaise Pascal, 77455 Marne La Vallée cedex 2, France

[b]Commissariat à l'énergie Atomique, DEN, DANS, DM2S, Université Paris-Saclay, F-91191 Gif-sur-Yvette, France

***Corresponding Author:**
Feng Zhang
Ecole des Ponts ParisTech
Laboratoire Navier, 6-8 av. Blaise Pascal, 77455 Marne La Vallée cedex 2, France
Email: feng.zhang@enpc.fr

© 2021 published by Elsevier. This manuscript is made available under the CC BY NC user license
https://creativecommons.org/licenses/by-nc/4.0/

Abstract

This study was aimed at highlighting the effect of loading frequency on the sand liquefaction response by performing cyclic triaxial tests in both stress-controlled and strain-controlled modes. For the first case, dense (I_{Dmat}=0.70) and medium-dense (I_{Dmat}=0.55) sand specimens were subjected to alternative and non-alternative axial stresses; whilst dense (I_{Dmat}=0.70) sand specimens were subjected to alternative axial strain over a wide range of loading frequencies in the second case. It was experimentally found that in the case of alternative loading for test specimens with I_{Dmat}=0.70 in stress-controlled mode, the effect of the loading frequency was not notable for dry sand specimens. In contrast, the effect of the loading frequency was significant for saturated sand specimens in both the loading modes. This was because, upon shearing, transient deformation occurred with the presence of excess pore water pressure, during which the inertia force needed to be taken into account. In the axial direction, the inertia force opposing the external loading certainly increased the liquefaction resistance by suppressing the complete development of the sand liquefaction. As for non-alternative loading in stress-controlled mode for test specimens with I_{Dmat}=0.55, the loading frequency played a vital role in pure extensional loading, which could also be logically attributed to the presence of the axial inertia force appearing in the large strain and transient deformation stages. However, the effect of the loading frequency on the compressive pattern was unclear due to the following two reasons: (i) the inertia force in the lateral direction appeared in the form of enhancing lateral confinement, thereby impeding the relative sliding; and (ii) during shearing, the rearrangement of the sand grains occurred in a more stable direction. These two aspects both provided beneficial contribution to sand liquefaction resistance, thereby preventing the occurrence of transient deformation. Under the circumstance, the sand specimens deformed only moderately, thereby eliminating the need to consider the role of the loading frequency.

Keywords: Sand liquefaction; Loading frequency; Cyclic triaxial tests; Alternative and non-alternative loadings

1. Introduction

Sand liquefaction has emerged as an engaging topic in geotechnical engineering since the occurrence of the Niigata earthquake in Japan [1] and Alaska earthquake in the United States [2]. Under seismic loading, liquefaction may result in catastrophic consequences (e.g., transient deformation) pertaining to above-ground structures and underground lifelines due to the rapid build-up of excess pore water pressure [3]. According to the "Seed-equivalent method" [4] that simplifies the recorded irregular earthquake shear stresses to an alternative equal-amplitude loading, the liquefaction potential has been commonly assessed by performing cyclic triaxial tests in laboratory research. Due to the inherent limitation of actuator devices, experimental work has been mostly conducted under a lower level of loading frequencies, for instance 0.05 Hz [5], 0.10 Hz [6–8], 0.20 Hz [9], 1 Hz [10,11] and etc., in order to better control the imposed loading, as well as overcome the measurement problems of the rapid excess pore water pressure and axial strain. However, the frequency of a real seismic excitation typically varies in the range of a few hertz [12–14], which indicates the effect of this element is also a pronounced parameter that needs to be underlined in laboratory tests [15].

Considerable research has been devoted to examine this aspect over the past fifty years. However, no clear consensus has been accomplished, and diverse views still exist in the published literature as to whether the commonly used lower frequency values are conservative or radical in the context of earthquake engineering. In general, the outcomes of earlier investigations revealed an ignorable effect of loading frequency [16–20] on the liquefaction response. For instance, a Roscoe-type simple shear device was applied by Peacock [16] to examine the liquefaction potential of medium-dense saturated Monterey sand under different loading frequencies within the range of 0.17-4 Hz. However, no clear tendency of the loading frequency was observed since the obtained experimental data dispersed within $\pm 10\%$ of the mean value. Similar results have also been reported by other investigators, including Yoshimi [17] and Tatsuoka [18,19], who performed ring torsion and cyclic triaxial tests on medium-dense Bandaijima and Toyoura sands, respectively. More recently, certain conclusions have been repeatedly derived, albeit in a seemingly at least controversial manner. For instance, a series of cyclic simple shear tests was carried out by Nong [21] on loose and dense specimens (density index I_d= 0.40 and 0.80, respectively) by varying the loading frequency from 0.05 to 1 Hz. The

experimental results showed that (i) the number of cycles to attain a given failure criterion increased with the loading frequency; and (ii) the accumulated excess pore water pressure decreased with the loading frequency. These two phenomena indicated a lower liquefaction potential under a higher loading frequency, which is in agreement with the other reports [22–26]. In contrast to this beneficial contribution of loading frequency to liquefaction resistance, Mulilis [27] seemed to be the first to observe a totally reversed trend that the sand specimen examined at a frequency of 0.017 Hz was approximately 20% more resistant than that at a frequency of 1 Hz. Similarly, Dash [28] demonstrated the enhancement of the cyclic resistance of original Ahmadabad sand with a decrease in the loading frequency.

Table 1 summarizes the references mentioned above and it can be noted that the divergence in the effect of the loading frequency seems not to be possibly attributed to the employed test method, density of the sand specimen or failure criteria to identify the initial liquefaction. Furthermore, in these studies, the majority of attentions were paid to assessing the alternative loading pattern, owing to which, the eventual mechanism in pure extensional and compressive cycles could not be completely addressed. For this purpose, the emphasis of this study was put on (i) performing stress-controlled cyclic triaxial tests on saturated sand specimens subjected to both alternative and non-alternative loadings in order to separate the possible responses in the extensional/compressive cycles from the integrated alternative ones; and (ii) performing strain-controlled cyclic triaxial tests over a sizable frequencies range (up to 5 Hz) in order to directly underline the dynamic deformation characteristics. In addition, dry sand specimens were also adopted in stress-controlled triaxial programme to clarify the sliding mechanism of the sand grains without the interaction of the pore water under different loading frequencies.

2. Material and methods

2.1. Physical properties of the test material

The sand used in this study is a poorly graded Hostun 31 sand (termed "HN31" hereafter), which is characterized by uniform sub-angular grains [6,29] and widely used in many laboratories in Europe. The grain size distribution curve of HN31 sand [29] determined through the laser diffraction method [30] is depicted in Figure 1. The principle of this method is that while passing through a laser beam, a particle could scatter the light at a certain angle and intensity linking to its grain size. The detailed index properties are listed in Table 2.

2.2. Cyclic triaxial test apparatus

One of the most important features required of the cyclic triaxial device for sand liquefaction analysis is that the vertical piston must be firmly connected to the upper triaxial base so as to generate two-way alternative loading, in which cyclic stress could reverse its direction from triaxial compression to extension and vice versa. In this work, an advanced cyclic triaxial device (Mono50kN [7,31]) developed in the Navier laboratory of Ecole des Ponts ParisTech was employed. The vertical actuator of Mono50kN is connected to a PID (Proportional-Integral-Derivative) controller. In stress-controlled mode, the test specimen could be further subjected to equal-amplitude alternative shearing on its 45° plane after attaining the isotropic consolidation state of K_c=1 (consolidation stress ratio, $K_c=\sigma'_a/\sigma'_r$) as that generated on the horizontal plane [32] on the ground during earthquakes. This is the basis on which the cyclic triaxial test is warranted as a meaningful approach to assess the sand liquefaction behaviour [33]. Near the final part of the test, the employed PID controller probably fails since total material softening occurs with sand liquefaction; accordingly, the applied loading frequency should be limited to a lower range. In strain-controlled mode, the test specimen is subjected to equal-amplitude cyclic axial strain in each loading cycle; as a result, the axial displacement of test specimen is exactly the same as the given imposed loading. In addition, very high loading frequency is achievable in this mode since the axial displacement is prescribed and irrespective of sand liquefaction softening.

2.3. Cyclic test programme

The test programme is summarized in Table 3. For stress-controlled tests, it should be mentioned that (i) in order to ensure a suitable scale for the number of cycles to well distinguish any possible behaviour from various deformation ranges, dense sand specimens with a density index of sand matrix I_{Dmat}=0.70 were sheared in a moderate alternative pattern of T_{cc}=0.22 (cyclic stress ratio $T_{cc}=\tau/\sigma'_c=\sigma_d/2\sigma'_c$, where τ, σ'_c and σ_d denote the shear, effective confining and imposed deviator stresses, respectively) in CTT1-7; and (ii) considering the fact that sand specimens normally become more resistant when subjected to non-alternative loading [6], as verified in the preliminary tests conducted in this work, high-level non-alternative extensional (CTT8-10) and compressive (CTT11-13) loading patterns with T_{cc}=0.60 were thus implemented on medium-dense sand specimens with I_{Dmat}=0.55 so as to (i) control the test duration to be in an acceptable range; and (ii) eliminate the need to consider any possible leakage of the fragile latex membrane in the long term. For strain-controlled tests, all test specimens (CTT14-18) underwent an imposed alternative strain in the axial direction with a peak value of ε_a=±0.40% and a very high loading frequency of f=5.00 Hz was included in the test programme for a better viewing of pure dynamic deformation characteristic, as explained previously.

The cylindrical specimen with a diameter and height of 100 mm and 200 mm, respectively, was fabricated with 10 layers and each layer was carefully introduced into a split mould followed by slight compaction efforts (e.g., dry tamping method [34]) to achieve the required thickness (20 mm) by using a hand-held tamper. Once the test specimen was generated, the top triaxial base was mounted and sealed with a water-tight O-ring. Subsequently, a slight vacuum of approximately 20 kPa was applied to minimize any possible disturbances while removing the split mould, as well as to check the leakage of the latex membrane. Before initiating the three-step saturation for the saturated specimen (e.g., CTT4-18), the confining pressure was increased to 100 kPa to maintain the test specimen. Carbon dioxide (CO_2) was firstly purged into the dry specimen to evacuate the air bubbles, followed by the injection of de-aired water to saturate the test specimen. Note that the flux of both the CO_2 and de-aired was minimized to avoid disturbing the soil fabric. Thirdly, in order to render the test specimen fully saturated, the back and confining pressures were alternatively increased in small steps of approximately 20 kPa until Skempton's B value ($B=\Delta u/\Delta\sigma_{con}$, where Δu and $\Delta\sigma_{con}$ denote the

variation in the excess water pressure and imposed confining pressure, respectively) was equal to or greater than 0.98, which is believed to be high enough for the saturation of sandy soil. As for dry sand specimens (e.g., CTT1-3), the confining pressure was also increased to 100 kPa without performing the aforementioned saturation step.

3. Experimental results

3.1. Repeatability test

Figure 2a and Figure 2b illustrate the evolutions of the deviator stress q with the axial strain ε_a and those of the excess pore water pressure Δu with the number of cycles N_{cyc}, respectively, with the two parallel specimens having identical test parameters (~~e.g.,~~ CTT6 in stress-controlled mode). It appears from Figure 2a that two stress-strain curves nearly coincided with each other; from Figure 2b that (i) before r_u (excess pore water pressure ratio, $r_u=\Delta u/\sigma'_c$) attaining a relatively high level of approximately 0.80, two curves were almost the same; (ii) beyond this point, certain differences were observed (e.g., $r_u>0.80$) owing to the fact that the vertical hydraulic actuator could not, at this stage, manage the transient variation of the axial displacement when the test specimen approached the liquefaction stage with a high accumulated value of Δu. Therefore, these two phenomena suggest that the test programme adopted in this study was deemed to be adequate with respect to the repeatability requirements.

3.2. Stress-controlled mode

3.2.1. Dry sand specimens subjected to alternative loading

Figure 3a shows the relationship between the axial strain ε_a and number of cycles N_{cyc} of the dry sand specimens (CTT1-3) subjected to alternative shearing of T_{cc} equal to 0.22 under distinct loading frequencies f of 0.02, 0.10 and 0.60 Hz. Although the minimum and maximum ε_a of dry sand specimens were quite small and of the order of approximately 10^{-3}, the corresponding amplitude of shear strain ($\gamma=(1+\nu)\varepsilon_a$, where ν denotes the Poisson's ratio) were still in excess of the threshold value of shear strain γ_{th} (typically around 10^{-4} [33]) on behalf of the initiation of the cyclic degradation in the elasto-plastic regime. Despite the fact that the loading frequency f was significantly increased by 30 times (from f=0.02 to 0.60 Hz), only a minor variation was recorded. This insignificant effect upon the loading frequency could not be possibly ascribed to the pure elastic behaviour of the dry sand specimen since plasticity (e.g., irreversible relative sliding of the sand grains) certainly occurred as explained previously~~($\varepsilon_a>\gamma_{th}$)~~.

Figure 3b presents the corresponding effective stress paths of the dry sand specimens. The three curves appeared to be nearly identical, reconfirming that the applied loading frequency

exerted a negligible effect on the dry sand specimens. It is interesting to note that although the drainage lines were definitively closed during shearing, the effective stress paths tended to follow a straight line with a slope of 3:1 (similar to those observed in triaxial drained tests), which indicated that neither excess pore water pressure nor excess air pressure occurred during shearing.

3.2.2. Saturated sand specimens subjected to alternative loading

The experimental results of saturated sand subjected to alternative shearing of T_{cc} equal to 0.22 under distinct loading frequencies f of 0.02, 0.10, 0.30 and 0.60 Hz (CTT4-7) are regrouped in the subplots of Figure 4. The imposed deviator stress σ_d acting on the test specimens sketched in Figure 4a suggests that prior to the triggering of the liquefaction response, the vertical hydraulic actuator remained able to generate the desired loading with a high robustness in the target range of loading frequencies (from f=0.02 to 0.60 Hz). The relationship between Δu and N_{cyc} depicted in Figure 4b shows that (i) the so-called "M line" [7,35,36] became increasingly notable while approaching r_u=1, indicating the occurrence of cyclic mobility of the dense sand specimen [6,7]; (ii) the applied loading frequencies played a vital role on the saturated sand response, compared with the dry sand specimens; and (iii) for a given number of cycles, Δu significantly increased as the loading frequency decreased. The relationship between ε_a and N_{cyc} depicted in Figure 4c suggests that (i) the observed strain range of the saturated specimens was dramatically larger than that of the dry sand specimens; (ii) in the initial phase of loading (e.g., $N_{cyc} \leqslant 10$), ε_a did not exhibit considerable fluctuations with the variation in the loading frequency; (iii) nevertheless, this difference became increasingly conspicuous with further loading after triggering transient deformation near the liquefaction stage; (iv) the number of cycles corresponding to the attainment of the considered failure criterion (e.g., ε_a=-3% in the single amplitude case) decreased with the decrease in the loading frequency. Note that the conventional failure criterion of ε_a=5% in the double amplitude case (or "peak-to-peak") for stress-controlled tests [33] was not employed in the present work since at a higher loading frequency, the generation of the desired loading pattern became extremely difficult, especially after the triggering of the liquefaction softening, particularly for f=0.60 Hz. Therefore, the failure criterion

of ε_a=-3% in the single amplitude was specially set as an alternative, allowing the test specimen to be evaluated with a higher level of confidence.

3.2.3. Saturated sand specimens subjected to non-alternative loading

Figure 5a describes the relationship between q and ε_a in the case of saturated sand subjected to non-alternative extensional loading (CTT8-10). Two different responses were observed: (i) in the initial loading phase, the three curves nearly coincided with one another; (ii) when subjected to further shearing, the test specimen deformed increasingly quickly and a notable dispersion was observed among the three curves while approaching the transient deformation stage. Figure 5b shows the corresponding evolution of Δu with respect to N_{cyc} and it can be seen that the Δu was initially positive due to the unloading volume-contraction effect (outlined through the purple circle) upon shearing. The same phenomenon has been previously reported and attributed to the reversible dilatancy by Li [37,38]. With further extensional loading, Δu steadily increased as cyclic axial stress was applied, and the specimen with lower f=0.02 Hz (marked in blue) tended to exhibit a slightly higher absolute value of Δu in both the phases (loading and releasing, as shown in Figure 5b) until the failure than that pertaining to the specimens with f=0.10 Hz (marked in red) and f=0.30 Hz (marked in green).

Figure 6a presents the relationship between q and ε_a in the case of saturated sand subjected to non-alternative compressive loading (CTT11-13). No clear impact of the loading frequency was observed. It is worth noting that as compared with that in non-alternative extensional loading, ε_a developed in a non-alternative compressive pattern under three distinct loading frequencies was deemed to be in a small range. Figure 6b shows the corresponding Δu in terms of N_{cyc}, and it can be seen that after the initial rapid increase, all the Δu were converged to approximately r_u=0.60 and the effect of the loading frequency could be considered to be trivial.

Figure 7 synthesizes the accumulated axial strain ε_a with respect to N_{cyc} under extensional (case a) and compressive (case b) loadings. In the first six loading cycles (as shown in Figure 7) in case a, no remarkable dispersion in ε_a was observed with the three loading frequencies. However, the strain rate continually (e.g., N_{cyc}>6) accelerated afterward, and the transient deformation was finally triggered. At this stage, the applied loading frequencies played a dominant role, indicating that a higher loading frequency (e.g., f=0.30 Hz) seemed to be able to

suppress the further development of ε_a. In case b, ε_a varied in a more moderate manner in all the loading ranges and finally stabilized to a certain level. In terms of the effect of the applied loading frequencies, only a minor variation was recorded, in contrast to that in case a.

3.3. Strain-controlled mode

3.3.1. Saturated sand specimens subjected to alternative loading

Figure 8 presents the experimental results of saturated sand subjected to alternative axial strain with ε_a=±0.40% (CTT14-18) under distinct loading frequencies f from 0.01 to 5.00 Hz. The stress-strain curves in Figure 8a show that the adopted PID controller functioned correctly as all axial strains fell within the prescribed range in relation to the imposed loading despite the significant increase in f. In terms of the deviator stress q, the amplitude value was much greater on the compression side than that on the extension side. This asymmetrical property is in accordance with the experimental observations reported in the literature [39]. The relationship between Δu and N_{cyc} depicted in Figure 8b shows that (i) with the first minor increase in f (from 0.01 Hz in blue to 0.02 Hz in red), two curves almost coincide with each other and no clear tendency upon f can be found; (ii) with the further huge increase (in particular to f= 1.00 and 5.00 Hz), the build-up of Δu remarkably decreased to be smaller with the increasing f. For strain-controlled cyclic triaxial tests, r_u is commonly taken as a reasonable yardstick to identify the onset of sand liquefaction [40], and a value of r_u=0.90 was thought in the present work. It can be seen from Figure 8b that N_{cyc} required to the attainment of this considered criteria increased with the increasing f, which is consistent with the observations in stress-controlled tests that the higher loading frequency could suppress the progress of sand liquefaction.

4. Discussion

For granular materials such as sandy soil, the overall soil resistance to deformation (e.g., axial stain in a cyclic triaxial test) beyond the elastic range is mainly the result of the irreversible sliding of the sand grains against one another, which leads to the generation of the occlusal friction represented by the reciprocal constraint of the adjacent sand grains on their relative movements. From a microscopic viewpoint, this occlusal friction (in Figure 9) between the sand grains could be determined considering the following two factors according to the friction law (f=$N\times\mu$): (i) the normal force N perpendicular to the contact point standing for the compaction degree of the sand grains, which can be globally represented by the effective confining pressure $\dot{\sigma}_c$ acting on the test specimen; and (ii) the fractional coefficient, μ, which can be represented by the intrinsic frictional angle of the sand used. Thus, it can be logically deduced that (i) for sand specimens composed of a given sand under a certain level of $\dot{\sigma}_c$, the occlusal friction against external loading can be assumed to be constant as long as relative sliding occurs; (ii) this occlusal friction is further irrespective of how fast [41,42] the relative sliding is. In the published literature, the experimental investigations conducted by Semblat [43] and Song [44] indicated an insignificant strain-rate effects on dry sand with stress magnitudes going up to 200 MPa and strain rates in excess of 10000/s [45]. This reason could explain why very similar responses were observed in the case of dry sand (e.g., CTT1-3), as shown in Figure 3.

The completely opposite phenomena (e.g., deformation range, effect of loading frequency) pertaining to dry (e.g., CTT1-3) and saturated sand specimens (e.g., CTT4-7 and CTT14-18) could be ascribed only to the saturation-dependency since all the other controlled parameters were exactly identical. In the alternative loading pattern, the imposed loading (σ_d in stress-controlled mode and ε_a in strain-controlled mode) could, in general, be divided into two different parts: (i) extension half cycles with q<0 and (ii) compression half cycles with q>0. In the former case, the test specimen was stretched due to the reduction in the deviator stress, owing to which, the test specimen exhibited a macroscopic necking form. In this process, for the saturated specimen, the sand grains slid away from one another. Consequently, the corresponding Δu was globally adjusted to be negative (as justified in Figure 5b) so as to maintain the total specimen volume as constant. In the latter case, the test specimen was compressed due to the increase in the deviator stress, owing to which, the test specimen exhibited a macroscopic barrel form. In

312 contrast to the extension cycles, the sand grains slid to approach one another, and the
313 corresponding Δu was adjusted to be positive (as proved in Figure 6b) so as to offset the volume-
314 contraction tendency. With regard to this fully saturated state, it should be considered that (i)
315 certain parts of the sand grains were likely suspended in the pore water and lost intergranular
316 contacts owing to the positive Δu, which facilitated the further generation of ε_a in the consequent
317 extension cycles; and (ii) the large degree of ε_a generated in the extension cycles promoted the
318 further rapid build-up of Δu in the consequent compression cycles. Under the abovementioned
319 reciprocal effects pertaining to the alternative cycles (compression with extension), an
320 increasingly enhanced softening liquefaction response may be expected. This aspect could
321 explain why under the same experimental conditions, the strain range of the saturated sand
322 specimens in stress-controlled tests was obviously more important than that of the dry sand
323 specimens. However, this argument could not legitimately elucidate the effect of the loading
324 frequency on the response of the saturated sand specimens (as shown in Figure 4) because the
325 sliding between the sand grains is still independent of the loading speed even under large ε_a. As
326 the time interval at which deformation occurs becomes very short in cyclic triaxial tests, it is to
327 be borne in the mind that inertia force of sand grains themselves is another kind of agency that
328 needs to be critically taken into account in the range of the transient deformation associated with
329 sand liquefaction. In general, the inertia force that characterizes the dynamic behaviour as
330 distinguished from the static one [33,45–47] depends on the (i) mass of the sand grains and (ii)
331 acceleration linked to the strain rate of the considered sand grains. Figure 10 schematizes a
332 conceptual model of the inertia force appearing in extension and compression half cycles,
333 respectively. In the axial direction, in the case of the extension cycles depicted in Figure 10a, the
334 inertia force appears opposite to the sand grains' movement, thereby enhancing the resistance to
335 the applied axial loading. In the case of the compression cycles, as shown in Figure 10b, the
336 presence of inertia force equally makes a beneficial contribution to the axial resistance in the
337 same manner. In other words, when the strain rate of the test specimen becomes conspicuously
338 important (e.g., in the case of transient deformation while approaching or attaining the
339 liquefaction response), the test specimen cannot experience a sufficient time lag, allowing the
340 full build-up of sand liquefaction to be achieved since the applied loading rapidly reverses its
341 direction in the cases of higher loading frequencies. This mechanism is capable to inhibit the
342 accumulated development of ε_a [48] in stress-controlled tests and Δu in strain-controlled tests. It

343 explains why a remarkable effect of the loading frequency occurred in saturated sand specimens
344 subjected to alternative loading. In this sense, a similar phenomenon should also be observed in
345 the case of dry sand specimens. However, the experimental results derived from Figure 3a do not
346 support this argument. This phenomenon might be attributed to the fact that without the presence
347 of Δu in the dry state, the deformation of dry sand grains can be considered as being quasi-static,
348 resulting in an ignorable effect of loading frequency.

349 For the lateral direction in the extension (see Figure 10a) and compression (see Figure
350 10b) cycles, two distinct mechanisms can be identified: the inertia force (i) exists in the form of
351 weakening the lateral confinement on the extension side and (ii) still makes a positive
352 contribution to the lateral confinement on the compression side. As explained in the foregoing
353 section, the relative sliding between the adjacent sand grains, yielding global resistance, is
354 proportional to the normal force N, as represented by the confinement level. Hence, the presence
355 of lateral inertia force in the compressive/extension cycles enhances and weakens the specimen
356 resistance to deformation, respectively. In addition, when the sand specimens are deposited
357 under gravity, it has been experimentally demonstrated [49,50] that the long axes of the sand
358 grains preferentially orient along the horizontal direction so as to achieve a naturally stable state.
359 Under pure compressive loading, the rearrangement of the sand grains occurs in a more stable
360 horizontal direction (e.g., barrel effect), whilst a totally reversed phenomenon could then be
361 expected for pure extensional loading (e.g., necking effect). By combining the above two factors,
362 it can be deduced that under the same level of loading (e.g, T_{cc}) with opposite loading directions
363 (compression versus extension), the resistance to deformation should be much more prevailing in
364 compressive loading than in extensional loading. This aspect could explain why a greater strain
365 range and transient deformation only occurred for test specimens subjected to non-alternative
366 extensional loading, during which the effect of loading frequency (experimentally justified by
367 Figure 5 and Figure 7) should necessarily be considered with the inertia force, as explained
368 previously. On the contrary, due to the lack of the above two key factors (considerably strain
369 range and transient deformation), the effect of the loading frequency (f=0.02-0.30 Hz employed
370 in the present work) could be logically assumed to be of second importance in the case of non-
371 alternative compressive loading, which is highly consistent with the experimental results
372 displayed in Figure 6 and Figure 7.

5. Conclusions

In this study, the effect of the loading frequency f was investigated by performing (i) stress-controlled cyclic triaxial tests for dry and saturated sand specimens in the dense (I_{Dmat}=0.70) and medium-dense (I_{Dmat}=0.55) states subjected to alternative and non-alternative loadings; and (ii) strain-controlled cyclic triaxial tests for saturated dense sand specimens (I_{Dmat}=0.70) over a wide range of f. The results can be used to derive the following conclusions:

1) Under alternative loading, dry sand specimens with I_{Dmat}=0.70 (CTT1-3) deformed almost in a quasi-static manner and were insensitive to the variation in f, which eliminated the need to consider the additional inertia force.
2) In the presence of pore water, the saturated sand specimens with I_{Dmat}=0.70 subjected to alternative loading indeed liquefied with transient deformation. In stress-controlled mode (CTT4-7), the effect of the f was required to be carefully considered, especially after the triggering of transient deformation associated with sand liquefaction. In strain-controlled mode (CTT14-18), a significant effect of f was also found when the applied f was drastically increased. In these two cases, the presence of inertia force opposing the applied loading in the axial direction is the main reason to explain the above experimental observations.
3) In the case of non-alternative loading in pure extensional loading for stress-controlled tests, a higher f also made a beneficial contribution to axial resistance for medium-dense saturated sand specimens with I_{Dmat}=0.55 owing to the presence of the axial inertia force, very similar to the alternative loading for saturated specimens in dense state (I_{Dmat}=0.70). In contrast, no clear effect of f was observed in the case of pure compressive loading, which could be ascribed to the following two factors: (i) the inertia force in the lateral direction appeared in the form of enhancing lateral confinement, thereby impeding the relative sliding; and (ii) during shearing, the rearrangement of the sand grains took place in a more stable direction. Therefore, the sand specimens only deformed in a moderate manner without transient defamation leading to an ignorable effect of the f.

Acknowledgements

The authors acknowledge the support of the geotechnical laboratory of Ecole des Ponts ParisTech. The financial support provided by the research sponsors through ANR ISOLATE and the inspiring discussion on dynamic issues with Dr. Li are deeply acknowledged.

406 Reference

407 [1] Ishihara K, Koga Y. Case Studies of Liquefaction In the 1964 Niigata Earthquake. Soils
408 Found 1981;21:35–52.

409 [2] Wyss M, Brune J. The Alaska earthquake of 28 March 1964: A complex multiple rupture.
410 Bull Seismol Soc Am 1967;57:1017–23.

411 [3] Ni X, Ye B, Ye G, Zhang F. Unique determination of cyclic instability state in flow
412 liquefaction of sand. Mar Georesources Geotechnol 2020;0:1–9.
413 https://doi.org/10.1080/1064119X.2020.1791289.

414 [4] Seed H, Idriss I, Makdisi F, Banerjee N. Representation of irregular stress time histories
415 by quivalent uniform stress series in liquefaction analyses. Berkeley: 1975.

416 [5] Benghalia Y, Bouafia A, Canou J. Comportement mécanique des sols sableux avec un
417 indice des vides intergranulaire constant. 8ème Colloq. Natl. afps, 2011.

418 [6] Benahmed N. Comportement mécanique d'un sable sous cisaillement monotone et
419 cyclique: application aux phénomènes de liquéfaction et de mobilité cyclique. Ph.D Thesis
420 Ecole Nationale Des Ponts et Chaussées, 2001.

421 [7] Jradi L. Study of the Influence of Fine Particles on the Properties of Liquefaction of Sands.
422 Ph.D Thesis University Paris-Est, 2018.

423 [8] Suzuki M, Yamamoto T. Liquefaction Characteristic of Undisturbed Volcanic in Cyclic
424 Triaxial Test. 13th World Conf. Earthq. Eng. Vancouver, 2004.

425 [9] Ghionna VN, Porcino D. Liquefaction resistance of undisturbed and reconstituted samples
426 of a natural coarse sand from undrained cyclic triaxial test. J Geotech Geoenvironmental
427 Eng 2006;132:194–202. https://doi.org/10.1061/(ASCE)1090-0241(2006)132.

428 [10] Sitharam TG, GovindaRaju L, Srinivasa Murthy BR. Evaluation of liquefaction potential
429 and dynamic properties of silty sand using cyclic triaxial testing. Geotech Test J
430 2004;27:423–9. https://doi.org/10.1520/gtj11894.

431 [11] Saxena SK, Reddy KR, Avramidis AS. Liquefaction resistance of artificially cemented
432 sand. J Geotech Eng 1988;114:1395–413.

[12] Silva WJ. Soil response to earthquake gound motion. 1988.

[13] Kramer SL. Geotechnical Earthquake Engineering. 1996.

[14] Boore DM, Bommer JJ. Processing of strong-motion accelerograms: Needs, options and consequences. Soil Dyn Earthq Eng 2005;25:93–115. https://doi.org/10.1016/j.soildyn.2004.10.007.

[15] Ye B, Xie X, Zhao T, Song S, Ma Z, Feng X, et al. Centrifuge Tests of Macroscopic and Mesoscopic Investigation into Effects of Seismic Histories on Sand Liquefaction Resistance. J Earthq Eng 2020;00:1–23. https://doi.org/10.1080/13632469.2020.1826373.

[16] Peacock WH, Seed HB. Sand liquefaction under cyclic loading simple shear conditions. J Soil Mech Found Div 1968:689–708.

[17] YOSHIMI Y, OH-OKA H. Influence of Degree of Shear Stress Reversal on the Liquefaction Potential of Saturated Sand. Soils Found 1975;15:27–40.

[18] Tatsuoka F, Maeda S, Fujii S, Yamada S. Cyclic Undrained Strengths of Saturated Sand under Random and Uniform Loading and Their Relation 1983.

[19] Tatsuoka F, Toki S, Miura S, Kato H, Okamoto M, Yamada S, et al. Some factors affecting cyclic undrained triaxial strength of sand. Soils Found 1986;26:96–116.

[20] Polito CP. The Effects Of Non-Plastic and Plastic Fines On The Liquefaction Of Sandy Soils. Verginia Polytechnic Institute and State University, 1999.

[21] Nong Z, Park S, Jeong S-W, Lee D-E. Effect of Cyclic Loading Frequency on Liquefaction Prediction of Sand. Appl Sci 2020;10:4502.

[22] Lee KL, Fitton JA. FACTORS AFFECTING THE CYCLIC LOADING STRENGTH OF SOIL. Vib Eff Earthquakes Soils Found 1969:71–95. https://doi.org/10.1520/STP33637S.

[23] Guo Y, He L. The Influences of the Vibration Frequencies on Liquefaction Strength of Saturated Sands. J Disaster Prev Mitig Eng 2009;29:618–22. https://doi.org/10.13409/j.cnki.jdpme.2009.06.015.

[24] Feng T, Zhang L. Experimental study on effect of vibration frequency on dynamic behaviors of saturatd sands. J Water Resour Archit Eng 2013;11:11-14,76.

460 [25] ZHANG S, ZHANG Y, ZHANG L, LIU C. Influence of Confining Pressure and Vibration
461 Frequency on the Liquefaction Strength of the Saturated Gravel Sand. J Xinjiang Agric
462 Univ 2015;38:68–71.

463 [26] Zhang J, Cao J, Huang S. Experimental Study on the Effects of Initial Shear Stress and
464 Vibration Frequency on Dynamic Strength of Saturated Sands. Adv Mater Sci Eng
465 2019;2019:1–9. https://doi.org/10.1155/2019/3758527.

466 [27] Mulilis JP, Chan, C K, Seed HB. The effects of method of sample preparation on the
467 cyclic stress-strain behavior of sands (EERC Report 75-18). University of California:
468 Berkeley, CA, USA: 1975.

469 [28] Dash HK, Sithara TG. Effect of frequency of cyclic loading on liquefaction and dynamic
470 preoperties of saturaed sand. Int J Geotech Eng 2016;10:487–92.

471 [29] Zhu Z, Dupla J, Canou J, Foerster E. Experimental study of liquefaction resistance : effect
472 of non-plastic silt content on sand matrix. Eur J Environ Civ Eng 2020;0:1–19.
473 https://doi.org/10.1080/19648189.2020.1765198.

474 [30] Yang J, Wei LM. Collapse of loose sand with the addition of fines: The role of particle
475 shape. Geotechnique 2012;62:1111–25. https://doi.org/10.1680/geot.11.P.062.

476 [31] Zhu Z, Zhang F, Peng Q, Chabot B, Dupla J. Development of an auto compensation
477 system in cyclic triaxial apparatus for liquefaction analysis. Soil Dyn Earthq Eng
478 2021;144:106707. https://doi.org/10.1016/j.soildyn.2021.106707.

479 [32] Zhu Z, Kham M, Fernandes VA, Lopez-Caballero F. Dynamic Response of a Central Clay
480 Core Dam Under Two-Component Seismic Loading. Springer Ser Geomech Geoengin
481 2020;1:231–6. https://doi.org/10.1007/978-3-030-46351-9_23.

482 [33] Ishihara K. Soil Behaviour in Earthquake Geotechnics. Oxford science publications; 1995.

483 [34] Zhu Z, Zhang F, Dupla JC, Canou J, Foerster E. Investigation on the undrained shear
484 strength of loose sand with added materials at various mean diameter ratios. Soil Dyn
485 Earthq Eng 2020;137. https://doi.org/10.1016/j.soildyn.2020.106276.

[35] Yoshimi Y, Tokimatsu K, Kaneko O, Makihara Y. Undrained Cyclic Shear Strength of a Dense Niigata Sand. Soils Found 1984;24:131–45. https://doi.org/10.3208/sandf1972.24.4_131.

[36] Evans M, Zhou S. Cyclic behavior of gravelly soil. Gr Fail Under Seism Cond ASCE 1994:158–76.

[37] Li G. Advanced Soil Mechanics. TsingHua University; 2004.

[38] Li G, Guo RP. Volume contraction in unloading of shear tests and reversible dilatation of soils. Chinese J Geotech Eng 2000;02:158–61.

[39] Kumar SS, Krishna AM, Dey A. Evaluation of dynamic properties of sandy soil at high cyclic strains. Soil Dyn Earthq Eng 2017;99:157–67. https://doi.org/10.1016/j.soildyn.2017.05.016.

[40] HAZIRBABA K, RATHJE E. A comparison between in situ and laboratory measurements of pore water pressure generation. 13th Wo, Vancouver: 2004, p. 1220.

[41] Xie DY. Soil dynamics. Beijing: Higher Education Press; 2011.

[42] Horn HM, Deere DU. Frictional characteristics of minerals. Geotechnique 1962;12:319–35.

[43] Semblat JF, Phong LM, Gray G. 3D-Hopkinson Bar: New Experiments for Dynamic Testing on Soils. Soils Found 1999;39:1–10.

[44] Song B, Chen W, Luk V. Impact compressive response of dry sand. Mech Mater 2009;41:777–85. https://doi.org/10.1016/j.mechmat.2009.01.003.

[45] Omidvar M, Iskander M, Bless S. Stress-strain behavior of sand at high strain rates. Int J Impact Eng 2012;49:192–213. https://doi.org/10.1016/j.ijimpeng.2012.03.004.

[46] Whitman RV, Healy KA. Shear strength of sands during rapid loadings. J Soil Mech Founadations Div ASCE 1962;88(SM2):99–132.

[47] Whitman R V. The response of soils to dynamic loadings. 1970.

[48] Aghaei Araei A, Reza Razeghi H, Hashemi Tabatabaei S, Ghalandarzadeh A. Loading frequency effect on stiffness, damping and cyclic strength of modeled rockfill materials. Soil Dyn Earthq Eng 2012;33:1–18. https://doi.org/10.1016/j.soildyn.2011.05.009.

[49] Oda M. Inital fabric and their relations to mechanical properties of granular material. Soils Found 1972;12:17–36.

[50] Yang ZX, Li XS, Yang J. Quantifying and modelling fabric anisotropy of granular soils. Geotechnique 2008;58:237–48. https://doi.org/10.1680/geot.2008.58.4.237.

519 Table and Figures

520 *Table 1 Summary of the literature review pertaining to the loading frequency effect*

No	Reference	Sand	Test Method	$\dot{\sigma_c}$ (kPa)	I_d	Failure criteria	f (Hz)	Frequency Effect
1	Peacock [16]	Monterey	SST(1)	500	0.50	r_u=1	0.17-4	minor
2	Yoshimi [17]	Bandaijima	RTT(2)	95.2	≈0.40	r_u=1	1-12	
3	Tatsuoka [18]	Toyoura	CTT(3)	98	0.50-0.80	ε_a=10% (DA(4))	0.05, 0.50	
4	Tatsuoka [19]	Toyoura	CTT	100	0.50	ε_a=10% (DA)	0.05-1	
5	Polito [20]	Monterey	CTT	100	0.74	r_u=1	0.50, 1	
6	Lee [22]	EI Monte and Silt	CTT	103	0.50, 0.75	ε_a=5%, 10% or 20% (DA)	0.17-1	stable at higher f
7	Guo [23]	NA(4)	CTT	100-300	0.28, 0.70	r_u=1	0.05-1	
8	Feng [24]	Fujian sand	CTT	50	0.30	r_u=1	0.05-2	
9	Zhang [25]	NA	CTT	100	0.65	r_u=1	0.50-2	
10	Zhang [26]	Wuchuan sand	CTT	50, 100, 150	0.55	r_u=1	1-3	
11	Nong [21]	Nakdong River sand	SST	50, 100, 200	0.40, 0.80	ε_a=7.5% (DA)	0.05-1	
12	Mulilis [27]	Monterey	CTT	100	0.50	ε_a=5% (DA)	0.017-1	stable at lower f
13	Dash [28]	Original Ahmadabad sand	CTT	100	0.54	r_u=1	0.10-0.50	

Note:(1) SST: simple shear test; (2) RTT: ring torsion test; (3) CTT: cyclic triaxial test; (4) DA: double amplitude
(5) NA: not available

521 *Table 2 Physical properties of the test material*

Material	D_{50} (μm)	C_u	e_{min}	e_{max}	G_s	I_p
HN31	350	1.57	0.656	1	2.65	Non-plastic

522

523 *Table 3 Cyclic triaxial test programme*

Reference	I_{Dmat} (1)		Loading Pattern	S_r (%) (6)	f (Hz)	Control mode	$\dot{\sigma}_c$ (kPa)	Waveform
		T_{cc} (2)						
CTT1					0.02			
CTT2	0.70	0.22	A (3)	0	0.10			
CTT3					0.60			
CTT4					0.02			
CTT5	0.70	0.22	A		0.10			
CTT6					0.30	Stress		
CTT7					0.60			
CTT8					0.02			
CTT9	0.55	0.60	NA(E) (4)	100	0.10			
CTT10					0.60		100	Sine
CTT11					0.02			
CTT12	0.55	0.60	NA(C) (5)		0.10			
CTT13					0.60			
		ε_a						
CTT14					0.01			
CTT15					0.02			
CTT16	0.70	±0.40%	A	100	0.10	Strain		
CTT17					1.00			
CTT18					5.00			

Note:(1) Density index of sand matrix: I_{Dmat}; (2) Cyclic stress ratio: T_{cc}
(3) Alternative loading: A; (4) Non-Alternative extensional loading: NA(E)
(5) Non-Alternative compressive loading: NA(C); (6) Saturation degree: S_r

524

525

526

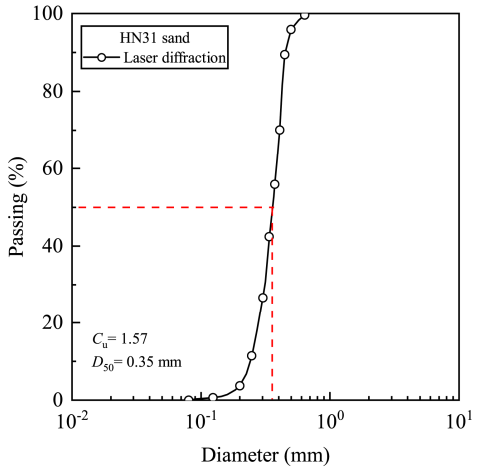

527

528 *Figure 1 Grain size distribution curve of HN31 sand.*

529

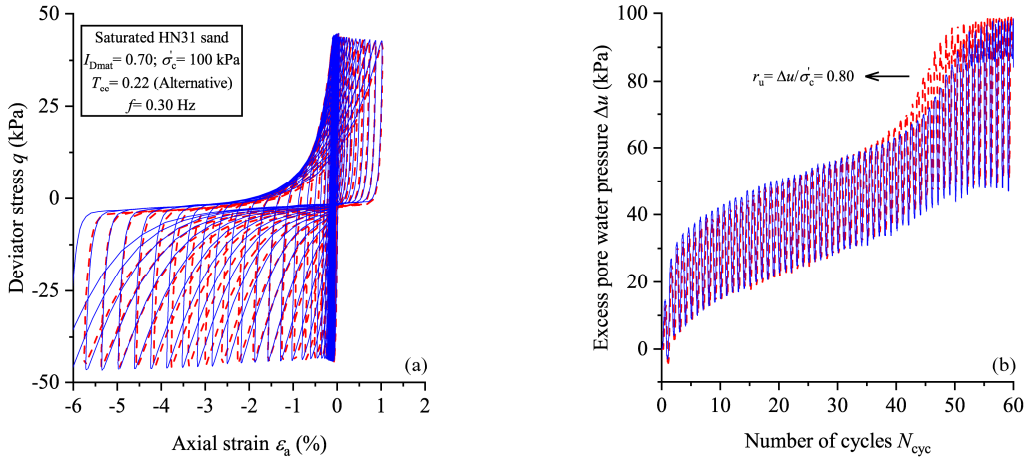

530

531 *Figure 2 Repeatability tests of specimens CTT6 with I_{Dmat}=0.70, $\dot{\sigma}_c$=100 kPa, T_{cc}=0.22*
532 *(Alternative) and f=0.30 Hz in terms of (a) stress-strain; and (b) excess pore water pressure-*
533 *number of cycles curves.*

534

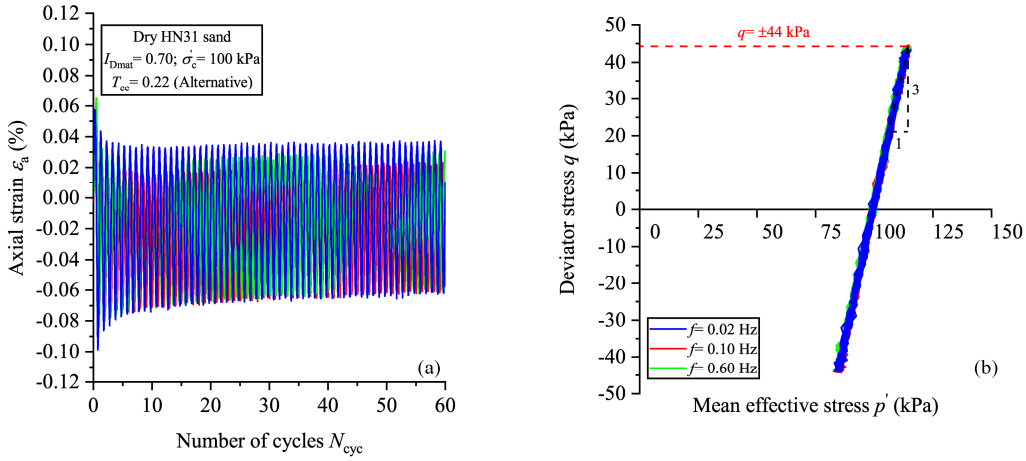

535

536 *Figure 3 Eexperimental results of dry sand specimens (I_{Dmat}=0.70, σ'_c =100 kPa) subjected to*
537 *alternative shearing (T_{cc}=0.22) under distinct loading frequencies (f=0.02, 0.10 and 0.60 Hz) in*
538 *terms of the (a) stress-number of cycles; and (b) effective stress paths curves.*

539

540 This figure is requested to be printed in color.

541

542

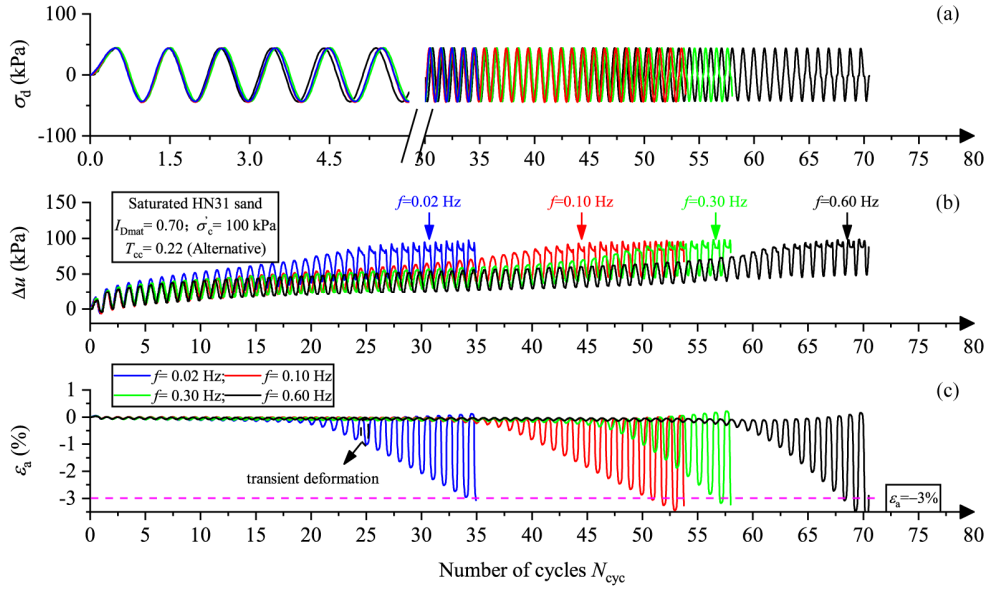

543

544 *Figure 4 Experimental results of saturated sand specimens (I_{Dmat}=0.70, σ'_c=100 kPa) subjected*
545 *to alternative shearing (T_{cc}=0.22) under distinct loading frequencies (f=0.02, 0.10, 0.30 and*
546 *0.60 Hz) in terms of the (a) deviator stress-; (b) excess pore water pressure-; and (c) axial*
547 *strain-number of cycles curves.*

548

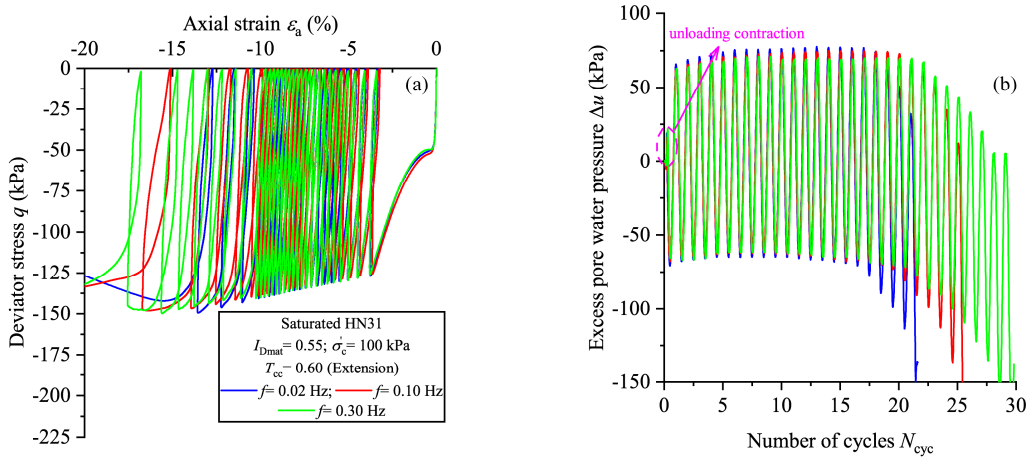

549

550 *Figure 5 Experimental results of saturated sand specimens (I_{Dmat}=0.55, σ'_c=100 kPa) subjected*
551 *to non-alternative extensional shearing (T_{cc}=0.60) under distinct loading frequencies (f=0.02,*
552 *0.10 and 0.60 Hz) in terms of the (a) stress-strain; (b) excess pore water pressure-number of*
553 *cycles curves.*

554

555 This figure is requested to be printed in color.

556

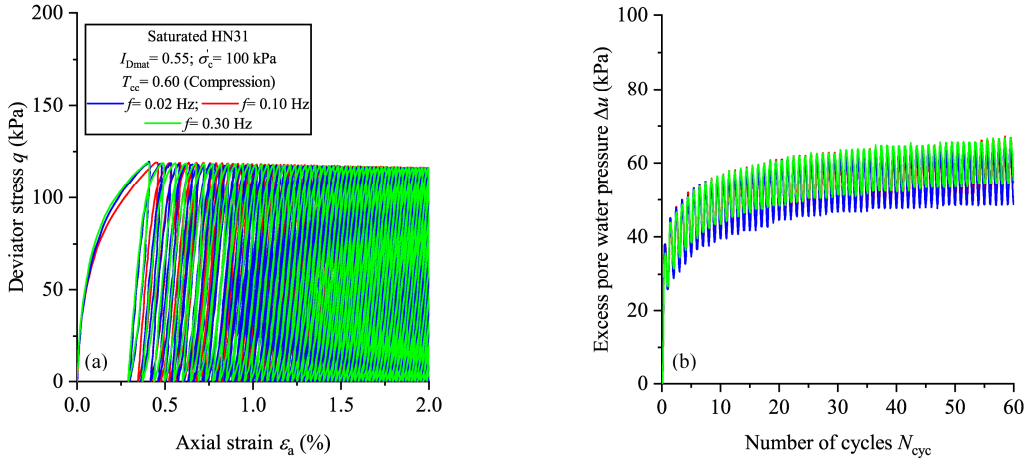

Figure 6 Experimental results of saturated sand specimens (I_{Dmat}=0.55, σ'_c=100 kPa, T_{cc}=0.60) subjected to non-alternative compressive shearing (T_{cc}=0.60) under distinct loading frequencies (f=0.02, 0.10 and 0.60 Hz) in terms of the (a) stress-strain; (b) excess pore water pressure-number of cycles curves.

This figure is requested to be printed in color.

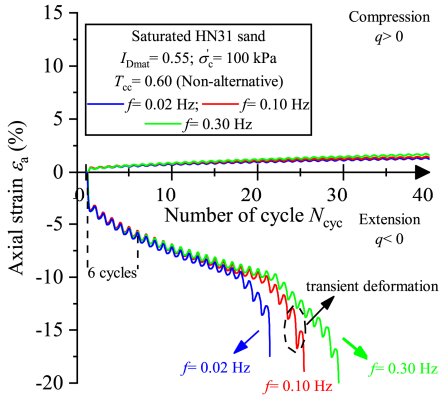

Figure 7 Accumulated axial deformation developed in the non-alternative loading of saturated sand specimens (I_{Dmat}=0.55, $\dot{\sigma}_c$=100 kPa, T_{cc}=0.60) on the (a) compression; and (b) extension sides.

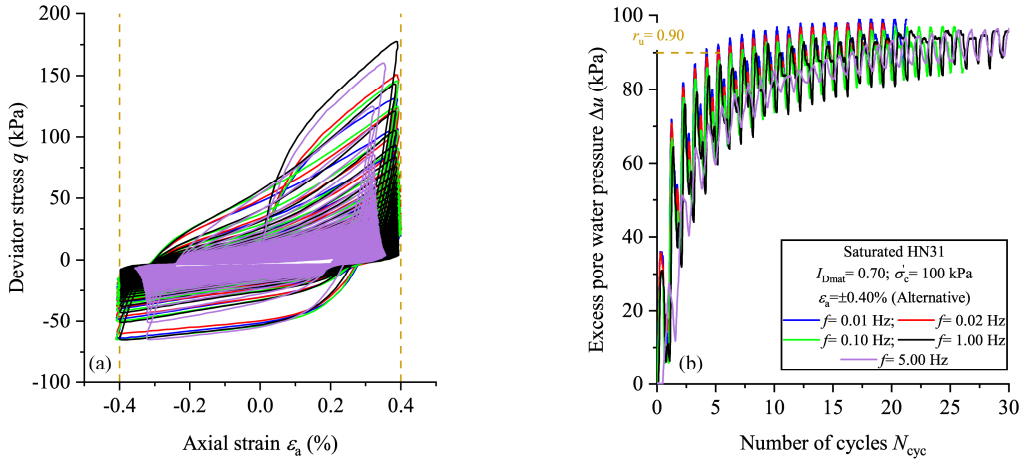

570

571 *Figure 8 Experimental results of saturated sand specimens (I_{Dmat}=0.70, σ'_c=100 kPa) subjected*
572 *to alternative axial strain (ε_a=±0.40%) under distinct loading frequencies (f=0.01, 0.02, 0.10,*
573 *1.00 and 5.00 Hz) in terms of the (a) stress-strain; and (b) excess pore water pressure-number of*
574 *cycles curves.*

575

576 This figure is requested to be printed in color.

577

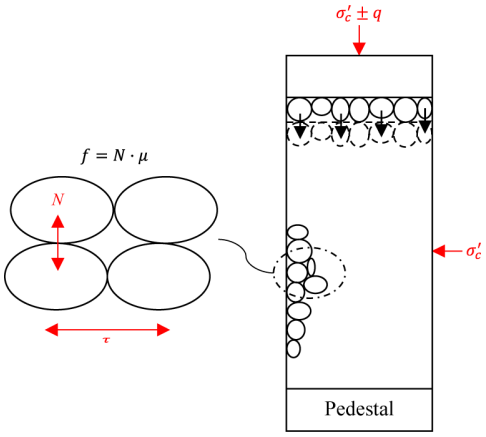

Figure 9 Schematic of occlusal friction of the dry sand specimen.

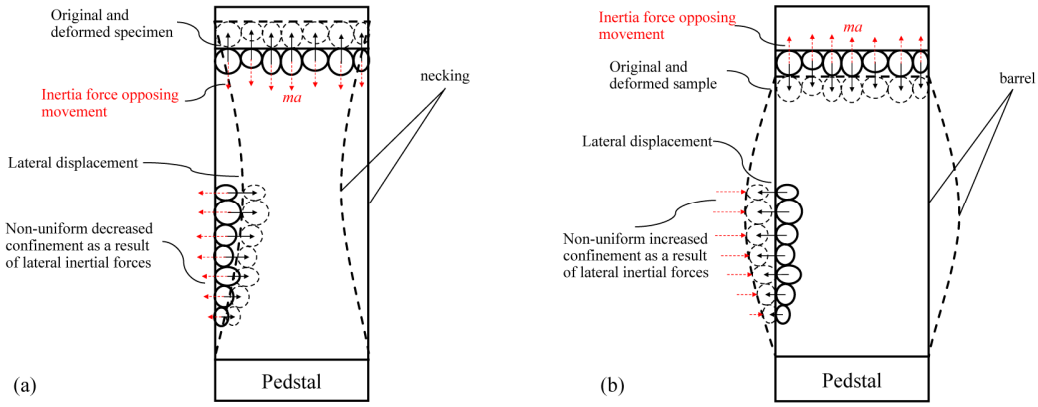

582

583 *Figure 10 Schematic of the inertia force in the (a) extension and (b) compression cycles*
584 *(modified from Omidvar* [45]*).*